*Journal of Seismology* **1:** 131–150, 1997.



# The $M_s$=6.2, June 15, 1995 Aigion earthquake (Greece): evidence for low angle normal faulting in the Corinth rift

P. Bernard[1], P. Briole[1], B. Meyer[2], H. Lyon-Caen[1], J.-M. Gomez[1], C. Tiberi[1], C. Berge[1], R. Cattin[1], D. Hatzfeld[3], C. Lachet[3], B. Lebrun[3], A. Deschamps[4], F. Courboulex[4], C. Larroque[4], A. Rigo[5], D. Massonnet[6], P. Papadimitriou[7], J. Kassaras[7], D. Diagourtas[7], K. Makropoulos[7], G. Veis[8], E. Papazisi[8], C. Mitsakaki[8], V. Karakostas[9], E. Papadimitriou[9], D. Papanastassiou[10], M. Chouliaras[10] & G. Stavrakakis[10]

[1] *Département de Sismologie, URA CNRS 195, Institut de Physique du Globe de Paris, 4 place Jussieu, 75252 Paris, Frnace;* [2] *Département de Tectonique, URA CNRS 1093, Institut de Physique du Globe de Paris, France;* [3] *Observatoire de Grenoble, France;* [4] *UMR Geosciences Azur, EP 125, CNRS-UNSA, Sophia Antipolis, France;* [5] *Observatoire Midi-Pyrénnées, Toulouse, France;* [6] *Centre National d'Etudes Spatiales, Toulouse, France;* [7] *Laboratory of Geophysics and Geothermy, University of Athens, Greece;* [8] *Dyonisos Observatory, Technical University of Athens, Greece;* [9] *Laboratory of Geophysics, University of Thessaloniki, Greece;* [10] *National Observatory of Athens, Greece*

Received 30 July 1996; accepted in revised form 20 May 1997

*Key words:* Normal faulting, Gulf of Corinth

**Abstract**

We present the results of a multidisciplinary study of the $M_s$ = 6.2, 1995, June 15, Aigion earthquake (Gulf of Corinth, Greece). In order to constrain the rupture geometry, we used all available data from seismology (local, regional and teleseismic records of the mainshock and of aftershocks), geodesy (GPS and SAR interferometry), and tectonics. Part of these data were obtained during a postseismic field study consisting of the surveying of 24 GPS points, the temporary installation of 20 digital seismometers, and a detailed field investigation for surface fault break. The Aigion fault was the only fault onland which showed detectable breaks (<4 cm). We relocated the mainshock hypocenter at 10 km in depth, 38° 21.7′ N, 22° 12.0′ E, about 15 km NNE to the damaged city of Aigion. The modeling of teleseismic P and SH waves provides a seismic moment $M_o$ = 3.4 $10^{18}$ N.m, a well constrained focal mechanism (strike 277°, dip 33°, rake −77°), at a centroidal depth of 7.2 km, consistent with the NEIC and the revised Harvard determinations. It thus involved almost pure normal faulting in agreement with the tectonics of the Gulf. The horizontal GPS displacements corrected for the opening of the gulf (1.5 cm/year) show a well-resolved 7 cm northward motion above the hypocenter, which eliminates the possibility of a steep, south-dipping fault plane. Fitting the S-wave polarization at SERG, 10 km from the epicenter, with a 33° northward dipping plane implies a hypocentral depth greater than 10 km. The north dipping fault plane provides a poor fit to the GPS data at the southern points when a homogeneous elastic half-space is considered: the best fit geodetic model is obtained for a fault shallower by 2 km, assuming the same dip. We show with a two-dimensional model that this depth difference is probably due to the distorting effect of the shallow, low-rigidity sediments of the gulf and of its edges. The best-fit fault model, with dimensions 9 km E–W and 15 km along dip, and a 0.87 m uniform slip, fits InSAR data covering the time of the earthquake. The fault is located about 10 km east-northeast to the Aigion fault, whose surface breaks thus appears as secondary features. The rupture lasted 4 to 5 s, propagating southward and upward on a fault probably outcropping offshore, near the southern edge of the gulf. In the shallowest 4 km, the slip – if any – has not exceeded about 30 cm. This geometry implies a large directivity effect in Aigion, in agreement with the accelerogram *aig* which shows a short duration (2 s) and a large amplitude (0.5 g) of the direct S acceleration. This unusual low-angle normal faulting may have been favoured by a low-friction, high pore pressure fault zone, or by a rotation of the stress directions due to the possible dip towards the south of the brittle-ductile transition zone. This fault cannot be responsible for the long term topography of the rift, which is controlled by larger normal faults with larger dip angles, implying either a seldom, or a more recently started activity of such low angle faults in the central part of the rift.

## 1. Introduction

The Gulf of Corinth has long been recognized as one of the most active rifts in the highly seismic Aegean. Its quaternary normal faulting (Sebrier, 1977), its high level of seismicity (Papazachos and Papazachos, 1989; Ambraseys, 1990), and the 1 cm/yr overall N–S geodetic extension rate (Billiris et al., 1991), makes it a key place within the Mediterranean area to study the physical processes related to the seismic cycle. Since 1991, a multidisciplinary Greek–French project based on extensive tectonic, geodetic, and seismic observations aims to better understand and model these processes in the Gulf area.

Although the Gulf has a long history of repeated earthquakes, few of the historical events have been unambiguously associated with a given fault. Extensive studies of the 1981 Corinth sequence surface breaks (Jackson et al., 1982; Hubert et al., 1996) and recent tectonic studies (Rigo, 1994; Armijo et al., 1996), however, indicate that the overall long-term morphology of the Corinth Rift is mainly due to repeated earthquakes on 40°–60° north-dipping prominent normal faults along the southern border of the rift (Figure 1). A two-month microseismic study conducted in the western part of the Gulf, near Aigion, revealed a strong clustering of microearthquakes, at 8–12 km in depth, suggesting that the steeply north-dipping normal faults root at these depths on a low angle dipping ($15 \pm 10°$) detachment zone (Rigo et al., 1996; Rietbrock et al., 1996). On the 15th of June 1995, an earthquake of magnitude 6.2 occurred in this area, which gave us a unique opportunity to understand the relationship between the seismic normal faulting and this active structure near the bottom of the brittle crust.

The 1995 Aigion earthquake struck the western part of the gulf of Corinth. It severely damaged the city of Aigion, on the southern shore of the gulf (2000 buildings sufferred major damage and had to be rebuilt), and killed 26 people in the collapse of two buildings. The earthquake was located by the National Observatory of Athens at 38.37° N, 22.15 E, about 12 km to the NNE of Aigion, under the northern coast of the Gulf. The Harvard solution (HRV, 1995) is an East–West striking, almost pure normal fault with a dip angle of 45° (Table 1); however, a recent, refined inversion provides a better constrained result, with an east–west striking, low angle nodal plane dipping 32° north (M. Nettles and G. Ekström, personal communication, 1997) (Table 1). The NEIC (National Earthquake Information Center, U.S.A.) mechanisms present a nodal plane dipping 35° towards the north, consistent with the revised Harvard solution (Table 1). With a magnitude $M_s$=6.2, this earthquake is the largest one recorded in the Gulf since the 1981 sequence which ruptured the eastern fault segments (Jackson et al., 1982) (Figure 1). It motivated a two-week seismotectonic field study starting two days after the earthquake, including the temporary installation of a seismological array for aftershock studies, the surveying of GPS points repeatedly measured in 1991–1994, and a detailed investigation for surface break along the well-known onshore active faults.

*Table 1.* Teleseismic source parameters of the 15 June 1995 Aigion earthquake.

| Source | Strike | Dip | Rake | $M_o$ (N · m) | h (km) |
|---|---|---|---|---|---|
| NEIC | 276° | 34° | −73° | $3.30 \cdot 10^{18}$ | 7 |
| HRV | 265° | 43° | −103° | $6.01 \cdot 10^{18}$ | 14 |
| Revised HRV | 287° | 32° | −78° | $5.1 \cdot 10^{18}$ | 10 |
| Body waves[a] | 277° | 33° | −76° | $3.4 \cdot 10^{18}$ | 7.2 |
| Body waves[b] | 278° | 28° | −71° | $2.5 \cdot 10^{18}$ | 7.2 |
| Body waves[c] | 272° | 38° | −82° | $4.9 \cdot 10^{18}$ | 7.2 |

NEIC, body wave solution; HRV, centroid moment tensor. [a] This work, best-fit model. [b] This work, low dip angle. [c] This work, large dip angle.

In this paper, we present the results of this field work, combined with the analysis of other data sets (inversion of teleseismic P and SH waveforms, mainshock relocation, and SAR interferogram modeling), for constraining the kinematics and geometry of the mainshock rupture. A major point of discussion is the identification of the ruptured nodal plane: the asymetry of the rift shows the dominant activity of north dipping faults, suggesting *a priori* the rupture of the low dip angle plane; however, mechanical arguments would *a priori* favour the rupture of the south-dipping, high angle plane, more consistent with usual friction laws. In any case, this earthquake appears atypical enough for justifying a carefull analysis of all the available data.

## 2. Tectonic observations

On the southwestern side of the gulf, where most of the damage occurred, three E–W striking *en echelon* normal faults (Psathopyrgos, Aigion, and Helike) mark the topography, and were *a priori* the most likely onshore faults to have produced the earthquake (Figure 1).

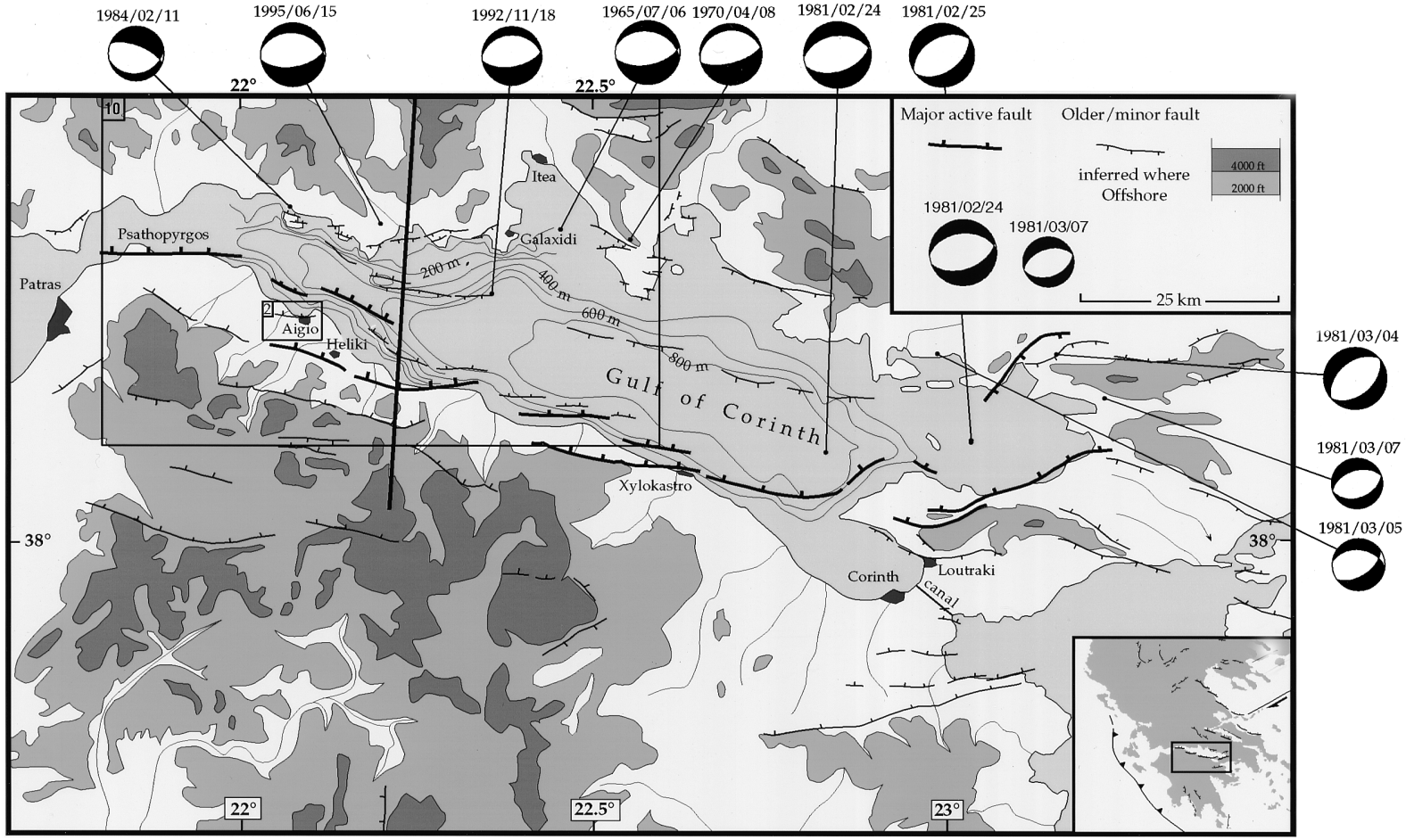


*Figure 1.* Active faults (from Armijo et al. (1996)) and major earthquakes since 1965 (1965, 1970: Baker et al., (1997); 1981, 1984: Taymaz (1990); 1992: location from the present study, mechanism from Hatzfeld et al. (1996); 1995: present study). The thick segment is for the cross-section of Figure 13.

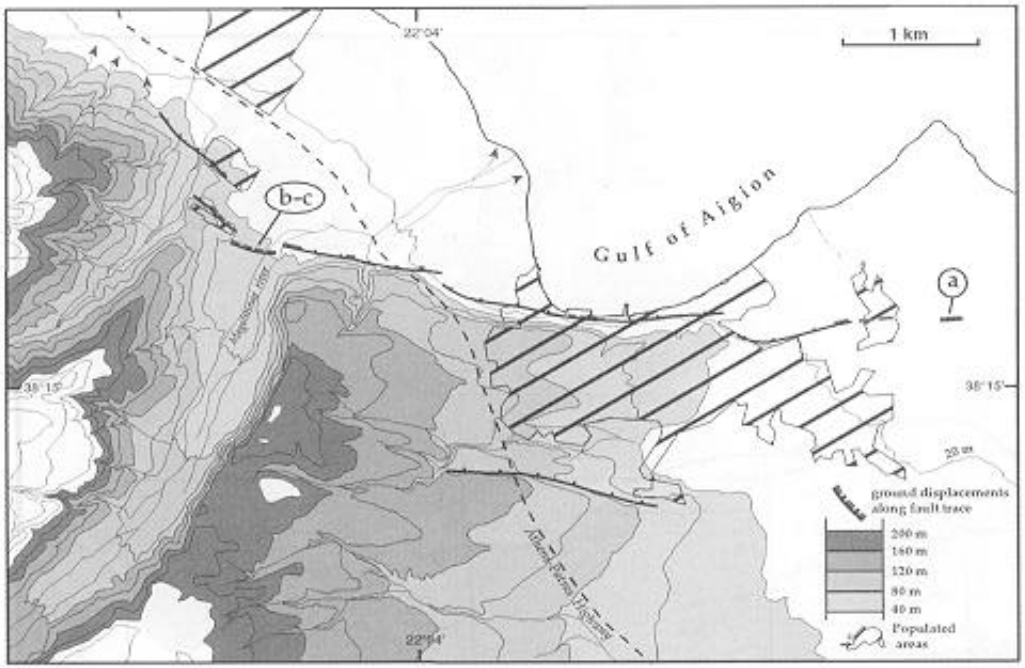


◀ *Figure 2.* Morphotectonic map of the Aigion normal fault. Topography (in m) from HAGS, (1980). Active fault trace from SPOT image (K-J 087/273), aerial photograph and fieldwork. Ground dislocation along fault traces from field observations. Arrows for location of photographs. a, b and c: location of sites in Figure 3.

*Figure 3.* Ground dislocation along fault trace during the June, 15, 1995 earthquake. (a) *N* 105°, 2 cm wide open cracks at the eastern end of the fault; (b) *N* 95°, open cracks across the road to Agios Constantinos on the left bank of the Meganeitas river. That the 20 cm high smoothed scarp on which open cracks are expressed formed during the earthquake remains unclear since local people testimonies disagree; (c) 2.5 cm wide fissure making a 3.5 cm high step 150 m westwards from b. ▼



The Psathopyrgos and Helike faults have onshore lengths of 12 and 18 km respectively, and outline the base of prominent cumulative fault scarps up to 400 m high. No historical earthquakes can be confidently related to the Psathopyrgos fault. On the other hand, the Helike fault, closer than the Psathopyrgos one to the area most severely damaged, is known to have been activated at least twice by large earthquakes during historical times in 373 B.C. (Mouyaris, 1992) and in 1861 (Schmidt, 1881; Mouyaris, 1992). The Aigion fault, on land 8 km long at most, appears as a secondary step within the right stepping Psathopyrgos and Helike faults. Although the Aigion fault has a subdued topographic signature and a cumulative fault scarp 80 m high at most, it is located within the epicentral region.

Since activation of any of the former faults cannot be ruled out, we carefully investigated the Psathopyrgos, Aigion, and Helike fault, as well as less prominent antithetic faults on the northern shore, searching for surface breaks at several key points along their traces. While clues of recent movements lack along the Psathopyrgos, the Helike, and the antithetic faults, surface displacements were observed in some places along the Aigion fault. The clearest ones occurred on a fairly continuous segment, 1.5-km-long, between the village of Agios Constantinos and the main tributary of the Meganeitas river. The break consisted of open fissures and small scarps with up to 4 cm of normal slip (Figures 2 and 3). No clear tectonic surface breaks were reported on the main fault segments whose long term morphology is the clearest (60–80 m high cumulative fault scarp), and on which the city of Aigion has been constructed. However, open cracks, parallel to the coast line, and fissures with a few centimeters of vertical displacement down to the north were observed 30 m away from the base of the fault scarp within the harbor. Towards the east, 1–3-m long open cracks were observed at the end and extending a smaller fault segment, with less prominent but still discernible morphology, cutting across the fan delta east of Aigion (Figures 2, 3a). That we could not find surface breaks all along the fault, and that the clearest ground dislocations at both ends of the fault trace occur in relatively flat areas filled with sediments (Meganeistas Valley, fan delta east of Aigion) cannot rule out a surficial effect of non tectonic origin. The very high ground acceleration in Aigion (0.5 $\boldsymbol{g}$ peak acceleration record on the NOA accelerometer) may indeed have induced the observed slip in the shallow part of the Aigion fault within recent alluvial deposits.

The only onshore fault candidate for possible surface breakage thus remains the Aigion fault, a secondary feature in terms of cumulative slip and uplift when compared with the Psathopyrgos and Heliki faults. A recent bathymetric survey of the gulf of Corinth has brought a much clearer image of the offshore active faults (Papanikolaou et al., 1996). Their preliminary results give evidence for large fault scarps (100-300 m meter of vertical throw) in quaternary sediments, north and east to Aigion, on both sides of the gulf: these faults might prove good offshore candidates for the 1995 rupture (Figure 1).

## 3. Location of aftershocks and relocation of the mainshock

The installation of a seismic network of 10 vertical and 10 three-component digital seismometers began three days after the mainshock (Figure 4a). Stations to the south were installed on the thick plio-quaternary marine sediments uplifted by the normal faults, whereas stations to the north were installed on hard rock (outcropping pre-tertiary limestone). Thousands of aftershocks were recorded every day. We used HYPO71 for locating the aftershocks in the 1D velocity structure provided by Rigo et al. (1996) for the western part of the Gulf of Corinth. A selection of the 800 best located events (6 P and 3 S phases) from 22 to 28 June 1995, is presented in Figures 4 (top) and 5. The time residual is less than 0.15 s, the standard horizontal and vertical errors are less than 1 km.

The aftershocks define an active zone about 20 km E–W and 10 km N–S, north to northeast to the Aigion fault, below the northern half of the gulf. They are mostly clustered between 5 and 9 km in depth (Figure 5). The shape and depth distribution of this nearly horizontal cluster of seismic activity is not very different from the microseismicity pattern drawn by the 1991 Aigion experiment (Rigo et al., 1996), nor by the aftershocks of the $M$ = 5.8, 1992 Galaxidi earthquake which occurred about 15 km to the east of the 1995 rupture (Hatzfeld et al., 1996). In the north–east, however, the aftershocks define a north dipping activity zone reaching 13 km in depth (Figure 5c). The absence of shallow activity reported in the southeastern part of the Gulf – in particular near the Aigion fault – might reflect the absence of shallow rupture in this area, but it might also result from a poor station coverage, and a higher seismic noise level of the southern sites located on thick plio-quaternary sediments. The absence of

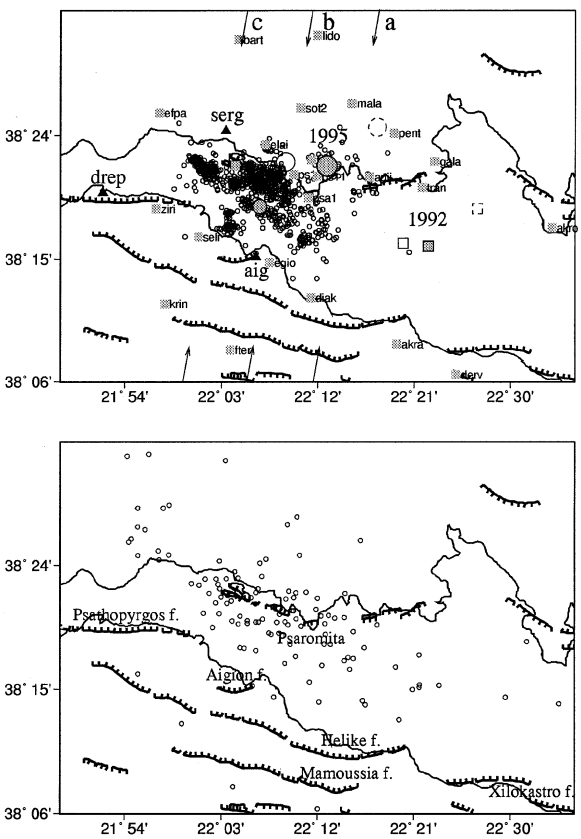


*Figure 4.* Aftershocks of the 1995 Aigion earthquake. (top) June 22–28. Small open circles: aftershocks. Shaded squares: digital seismometers of the 1995 temporary array. Filled triangle: strong motion accelerometers. Large open circle: NOA epicenter of the 1995 mainshock. Large dashed circle: NEIC epicenter of the 1995 mainshock. Large shaded large circle: relocated 1995 epicenter (this study). Shaded small circle: epicenter of the 1995 main aftershock (15 June, 03:30). Open square: NOA epicenter of the Galaxidi 1992 earthquake. Open dashed square: NEIC epicenter of the Galaxidi epicenter. Shaded square: relocated epicenter of the 1992 earthquake (this study). Arrows (a, b, and c): median position of the cross-section in Figure 5. (bottom) June 15 to 17 aftershocks, modified from Tselentis et al. (1996) (see text). Active faults from Armije et al. (1996).

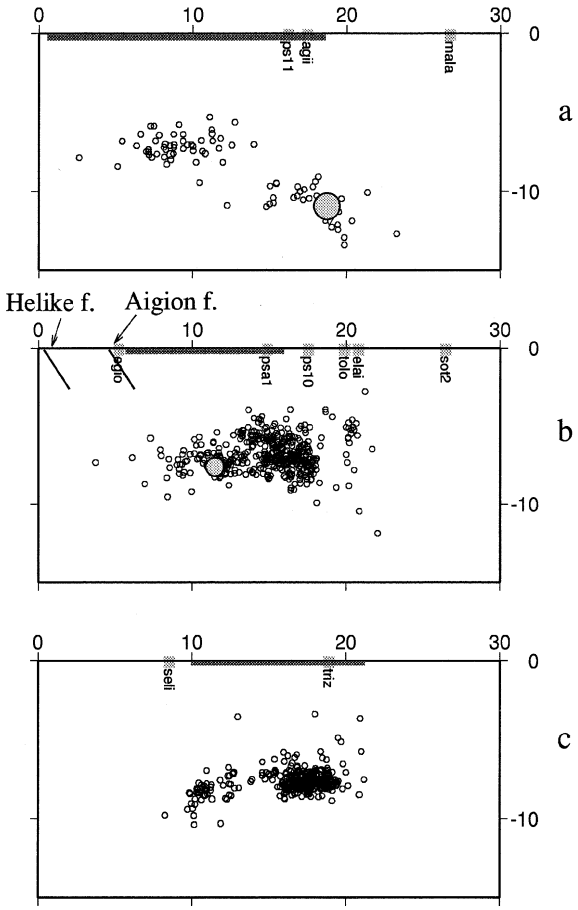


*Figure 5.* Same aftershocks as in Figure 4 (top), in the vertical cross-sections a, b, and c. Scale in km. Large shaded dot: relocated hypocenter of the 1995 mainshock. Small shaded dot: hypocenter of the 1995 main aftershock (depth inferred from aftershock cluster). Shaded area: gulf of Corinth. Width of the projections: 8 km.

reported shallow activity under the northern coast is much more significant, owing to a much denser station coverage and to much better site qualities (limestone) than on the southern coast.

In order to have a better estimate of the mainshock epicenter location, we used well located aftershocks from the temporary network to estimate systematic delays for the first arrival at the sites of the NOA national seismological network, and in addition we included S–P time delays from three local strong motion records. We selected the 5 best located events of our temporary network, as detailed in Table 2. They are all within 10 km from the mainshock epicenter. We calculated the theoretical first arrival times at the stations of the NOA national array with HYPO71, using the same layered structure as for the temporary network. The residuals at stations *rls* and *evr* are very small (0.1 to 0.2 s), and quite stable. For stations at larger distances, these residuals become larger (up to 1 to 2 s), reflecting the unsuitability of the velocity model (velocities are over-estimated), but, more important, they become quite variable, probably due to the difficulty to accurately pick refracted waves of such small events. Therefore, for some stations (*ath*, *kzn*, *plg*, *vam*, and *nps*), no reliable station correction could be proposed. We thus mainly relied on the *rls* and *evr* stations, and with a smaller weight on *itm*, *vls*, and *vli*.

*Table 2.* P time residuals (in s) at stations of the NOA seismic array for selected aftershocks

| Date June 1995 | East | North | Depth (km) | *rls* | *evr* | *itm* | *vls* | *ath* | *vli* | *kzn* | *plg* | *vam* | *nps* |
|---|---|---|---|---|---|---|---|---|---|---|---|---|---|
| 21 01:03 19.58 | 22° 8.37′ | 38° 19.47′ | 6.6 | 0.18 | −0.24 | −0.11 | −0.018 | 1.25 | −0.41 | −0.14 | −1.84 | −2.06 | |
| 21 02:24 26.27 | 22° 7.35′ | 38° 18.4′ | 8.0 | 0.36 | −0.11 | −0.33 | −0.17 | 0.85 | −0.57 | −0.12 | −1.72 | −3.15 | |
| 22 07:08 27.52 | 22° 0.55′ | 38° 22.25′ | 7.8 | −0.03 | 0.10 | 0.56 | 0.03 | 0.62 | 0.85 | 1.78 | −2.54 | | |
| 22 14:28 51.50 | 22° 6.73′ | 38° 20.94′ | 7.2 | −0.24 | −0.05 | −0.52 | −0.21 | 1.43 | −1.08 | 1.35 | | | |
| 23 14:32 52.96 | 22° 11.18′ | 38° 16.15′ | 7.5 | 0.38 | 0.22 | −0.56 | −0.80 | 1.62 | −0.27 | 2.04 | −2.35 | 7.04 | |
| Distance (km) to mainshock | | | | 72 | 70 | 133 | 142 | 140 | 194 | 219 | 248 | 373 | 459 |

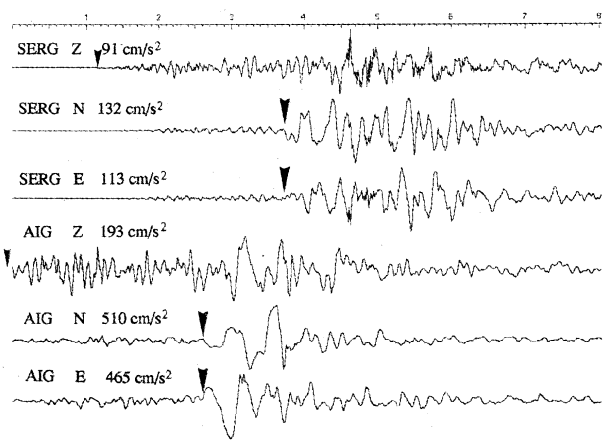


*Figure 6.* Acceleration records at *serg* and *aig* (see Figure 4, top). Peak values are indicated for each component. Z is vertical positive up. Small (resp. large) arrow for first P (resp. S) wave arrival. Time in s.

We used three local strong motion records. Two were obtained by the K2 accelerometers installed by the University of Athens (stations *serg* and *drep* of the RASMON network), and one was obtained on a SMA1 accelerometer installed by the National Observatory of Athens (station *aig* of the national network) (filled triangles in Figure 4a). The *aig* and *serg* records are plotted in Figure 6. The S–P time delay is accurately picked on the digital waveform for *serg* and *drep* (2.58 s and 4.34 s, respectively). For *aig*, as there is no pre-event memory, we estimated the S-P delay to be quite close to and minimized by the delay of the S arrival after the triggering (2.80 s).

We ran several times the HYPO71 program, with various weights to the stations: with or without the *aig* estimated S–P time; with higher or equal weights for the accelerometer S–P phases with respect to the nearest NOA stations; with low or zero weight to the furthest NOA stations. The various resulting epicentral locations are very stable, clustered within less than 1 km around 38° 21.7′ N, 22° 12.0′ E, with a typical rms of 0.24 s. The true epicentral uncertainty is estimated to be of the order of 2 km, when including the uncertainty in the velocity structure. The epicenter is thus shifted about 5 km west–southwest from the NOA original location. When looking at the corresponding cross-section of the aftershock activity, the epicenter falls at the northern limit of the main cluster. The depth is found between 10 and 11 km, with an uncertainty of 3 km, and is in reasonable agreement with the depths of the aftershocks in the eastern profile (Figure 5a).

We also redetermined the location of the $M_l$=5.2, main aftershock, which occurred 15′ after the mainshock. We applied the same procedure as for the mainshock relocation, using the first arrival phases of the NOA national array at (*rls, evr, itm, vls, vli*). The resulting location is 38° 18.46′, 22° 6.64′, plotted as a shaded circle in Figure 4 (top). It predicts an S–P delay of 2.17 s at *aig*, consistent with the observed S arrival time 2.3 s after triggering at this site.

When compared to the results obtained by Tselentis et al. (1996) with the records of the Patras telemetered array, our location of the mainshock and of the aftershocks cluster present a systematic shift to the NE, by several kilometers. We simply explain this difference by the fact that all the aftershock activity is located outside the Patras array, leading to this systematic biais in location. We applied a first order correction to the aftershock locations by Tselentis et al. (1996) by assuming that the spatial shift was the same for all the located events, including the mainshock. Our epicentral determination for the latter is 3.1′ to the north and 3.2′ to the east from the epicenter from Tselentis et al., which gives a 7 km shift. The effect of the correction on the aftershock location is plotted in Figure 4 (bottom)

for the first 3 days after the mainshock. As the two epicentral determinations of the main aftershock are within 4 km, we estimate the error in relocation to be 4 km. Figure 4 thus shows that some aftershock activity occurred southeast to the mainshock epicenter during the first three days, then dying out and clustering in its soutwestern quadrant.

## 4. Teleseismic body-wave modeling

To evaluate the range of allowable fault parameters, in particular for the dip, we analyzed the very broad-band digital data recorded by IRIS and GEOSCOPE networks for the 1995 Aigion mainshock, by simultaneously inverting P and SH waveforms for fault plane solution parameters, depth, seismic moment, and source time function. Seismograms recorded at epicentral distances of $31^\circ \leq \Delta_P \leq 89^\circ$ and $30^\circ \leq \Delta_{SH} \leq 87^\circ$ are used to carry out waveform modelling (Nábělek, 1984). Anelastic attenuation along the path is applied with a ratio of travel time to average quality factor (Q) of 1 s and 4 s for P and SH waves, respectively

We introduced a near-source structure based on the layered model of Rigo et al. (1996), and a half space at the receiver ($V_p$ = 5.6 km $\cdot$ s$^{-1}$, $V_s$ = 3,2 km $\cdot$ s$^{-1}$, $\rho$ = 2.6 gr $\cdot$ cm$^{-3}$, and a Poisson ratio of 0.25). We equalized seismograms to a common epicentral distance, and we weighted down the SH records to give the same significance to P and SH amplitudes (Nábělek, 1985). Velocity records were filtered by using band-pass Butterworth filter with cutoffs at 0.005 Hz and 0.5 Hz. We inverted a 20 s time window from the seismograms.

We assumed a simple point source, and the inversion provided the final best-fit solution: $\phi$ = 277°, $\delta$ = 33°, $\lambda$ = $-76^\circ$, $h$ = 7.2 km, and seismic moment $M_0$ = 3.38$\cdot 10^{18}$ N$\cdot$m, independent of the starting model. Focal solution, P and S seismograms, and source time function are shown in Figure 7a. For the best fit model, the source consisted in a first, major event lasting 4–5 s, possibly followed by a second, smaller moment release, 7 s after the beginning of the first event. However, this second event is much less reliable, as it is in the coda of the first direct waves, and contributes to less than 20% of the total moment.

In order to estimate the true resolution in dip angle, we ran the inversion with a fixed dip and left free the other parameters. The best-fit sources found for dip angles of 28° and 38° are plotted in Figure 7b and 7c, respectively (Table 1): both results provide

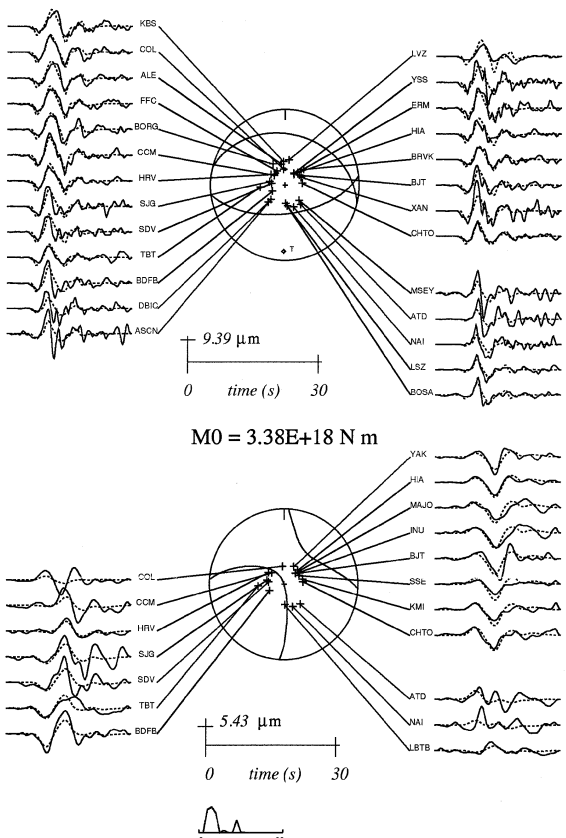


*Figure 7a.*

a poor fit to the data. For a dip of 28°, P waves at stations MSEY, ATD and NAI are almost nodal and their predicted amplitudes are too small. For a dip of 38°, the predicted first P down swing at all stations is larger than the observed; more globally, the predicted P amplitudes are too large, and the predicted S are too small.

The variance dependence on dip angle is presented in Figure 8 (left pannel, dots): the acceptable dip range is 25–35°, corresponding to a seismic moment range 2.7–4.0$\times 10^{18}$ N.m. The point source depth resolution is illustrated in Figure 8 (left panel, stars) the acceptable range is 6–7.5 km in depth.

We modeled the directivity effect of a propagating point source on the north dipping nodal plane (identified as the fault plane by the GPS data, as shown later). We explored all azimuths with a rupture velocity of 2.56 km$\cdot s^{-1}$ ($V_r = 0.8 \cdot \beta$) and we found a preferred propagation in the N240° direction (150° $-$ 350°), which is compatible with the epicenter location to the

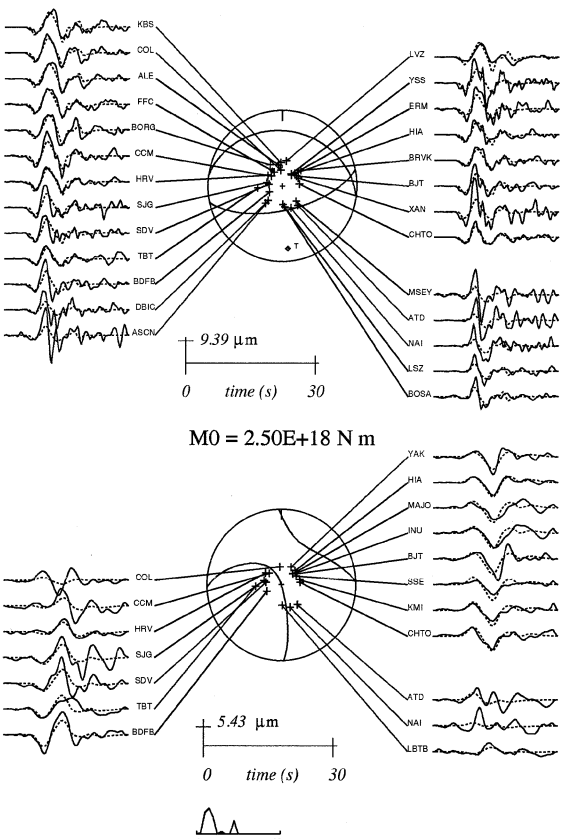


*Figure 7b.*

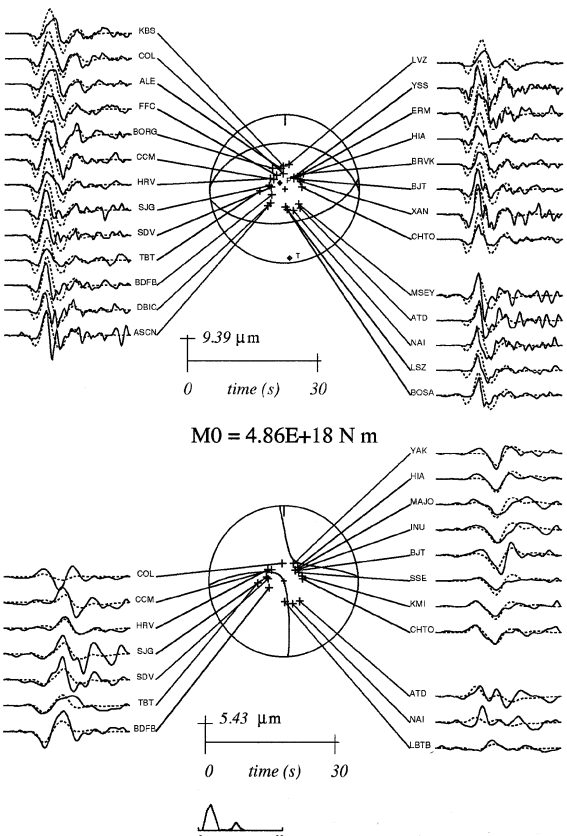


*Figure 7c*

*Figure 7.* Best fit focal mechanism and source time function from joint inversion of the P (top) and SH (bottom) teleseismic waves for a single point source at 7.2 km in depth. (a) all parameters free; best-fit dip 33°; (b) fixed dip 28°; (c) fixed dip 38°. Full line: data; dotted line: synthetic.

north-northeast of the activated fault plane and with an upward, southwestward propagation (Figure 8, right).

## 5. Near-source, S-wave polarization modeling

We analyzed the S-wave polarization of the mainshock recorded at the two closest accelerometers, *aig* and *serg*, in order to constrain the focal mechanism (see, e.g., Bernard and Zollo (1989); Zollo and Bernard (1991)). At *serg*, the shear-wave splitting detected by Bouin et al. (1996) gives less than 0.05 s of delay between the fast and slow S-wave: low-pass filtering the record at 1 Hz thus ensures the suppression of the anisotropy perturbation on the direct S-waves (Figure 9, top). At *aig*, no detailed study has been carried yet on the local anisotropy. The first S for the 1995 mainshock is polarized WNW–ESE, thus in agreement with the other fast S directions around the Gulf found by Bouin et al., (1996); the delay between split S is however difficult to determine, and possibly larger than 0.15 s.

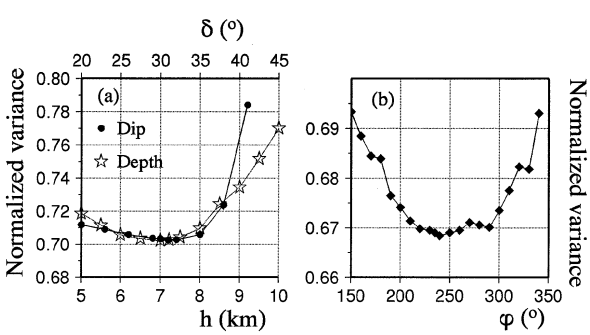


*Figure 8.* Resolution in depth, dip and directivity. (left) P and SH waveform modeling misfit versus dip angle $\delta$ (dots) and depth h (stars) for a point source. (right) misfit for a line source propagation in the $\varphi$ azimut (see text).

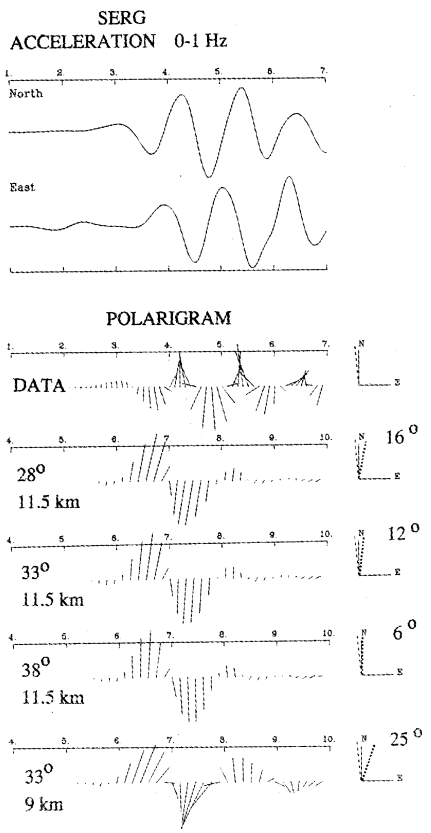


*Figure 9.* (top) horizontal components of the 0–1 Hz band-pass filtered acceleration at *serg* and associated polarigram (DATA) in the N,E plane. (bottom) synthetic polarigram for various hypocentral depths and fault dip angles (numbers to the left). The dashed (resp. dotted) line in the (N,E) quadrant is the mean observed (resp. synthetic) polarization for the first two seconds of S wave (DATA, 3–5 s). Angular difference is indicated to the right. The polarity (sign) of the first S pulses is not considered, being dependent on unresolved details of the slip history.

The resulting uncertainty in the local anisotropy effect lead us to exclude the *aig* record for a polarization analysis.

We used the 'k-square', kinematic source model of Herrero and Bernard (1994) for predicting the S-wave polarization at *serg*. This model assumes a circular rupture front propagating on a fault plane with a slip distribution following a *k-square* wavenumber spectral decay. The latter characteristics, which produces an $\omega$-square spectral decay of the body-wave, is not of crucial importance here as we are only looking for the low-frequency polarization of direct S-waves. We considered the velocity structure proposed by Rigo et al. (1996), replacing the first hundred meters by a low-velocity layer in order to reproduce the observed small incidence angles of P and S waves ($\beta$=1 km/s).

The fault plane is asssumed to be the north dipping nodal plane of the teleseismic inversions (see following paragraph), with a strike 277° and a rake −75°. The *a priori* fault location and size is consistent with the geodetic data (see following paragraph). It is 10 km in the NS direction, and 20 km in the EW direction. Its western limit, to which the record at *serg* is most sensitive, coincides with the limit provided by GPS data inversions. The assumed epicenter is 38°21.7, 22°12.0. We further assumed a rupture velocity of 80% of the shear-wave velocity, and a maximal rise-time of 0.3 s (corresponding to a pulse length of 1 km, see Bernard et al., 1996).

We tried several parameters for the dip (range 23–38°) and the hypocentral depth (range 8.5–11.5 km). For each trial depth, the predicted low-pass filtered S-polarization provides a better fit for the largest dip angle. For the 33° dip angle, the deepest focus at 11.5 km provides the best fit, with an error of 12°. Examples of the dip and depth sensitivity is given in Figure 9. With an acceptable error threshold of 20°, the S polarization analysis thus provides an independent constraint on the focal parameters: it excludes very low dip angles (below 25°) and shallow hypocentral depths (less than 10 km).

## 6. GPS measurements and SAR interferogram

Thirty-five geodetic points from the Corinth GPS network (established between 1991 and 1993) have been re-occupied between June 17 and June 24, 1995, using Ashtech and Leica dual-frequency GPS receivers. Twenty one first order points were occupied for about 8 hours three times and eleven second order points for 2–3 hours once or twice, following the same strategy as during the previous campaigns. The 24 best located points are indicated in Figure 10. The 1995 data were processed using the version 3.5 of the Bernese GPS Processing Software (Rothacher et al., 1993) and precise orbits. The internal accuracy of the coordinate determination is about 4 mm in the horizontal and 20 mm in the vertical, as given by the output of the adjustment of the daily determinations. This value is similar to that of the previous campaigns. The 1995 coordinates were compared with the coordinates the most recently obtained at the same points during previous surveys: October 1994 for points A, B, C, D, E, G and CT (processed using the same software as for the

*Table 3.* Fault models for the GPS and InSAR data

| Fault | East | North | Strike | Dip | Rake | Length (km) | $h_{\min}$ (km) | $h_{\max}(km)$ | Slip (m) | $M_0$ |
|---|---|---|---|---|---|---|---|---|---|---|
| A | 22° 13.2′ | 38° 16.9′ | 275° | 35° | −83° | 15 | 4.5 | 9.7 | 0.87 | 3.9 $10^{18}$ N.m |
| B | 22° 13.2′ | 38° 16.9′ | 275° | 35° | −83° | 15 | 2.5 | 7.7 | 0.87 | 3.9 $10^{18}$ N.m |

The coordinates refer to the projection at the surface of the centre of the upper edge of the fault. $h_{\min}$ is the depth of the upper edge of the fault and $h_{\max}$ the depth of the deeper edge of the fault.

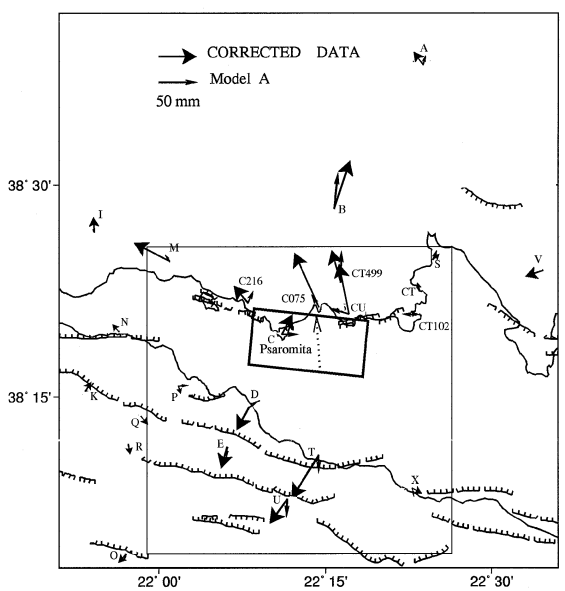


*Figure 10a.*

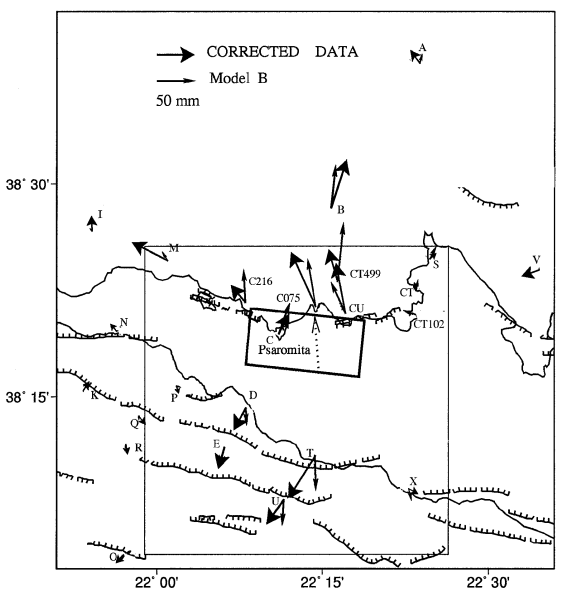


*Figure 10b*

*Figure 10.* GPS displacement modeling for the 15 june 1995 earthquake. Thick arrow: GPS data corrected from the secular trend. Thin arrow: modelled displacement with an elastic homogeneous half-space. The surface projection of the model fault (dipping 35° north) is shown as a small rectangle. The dotted arrow gives the slip direction. The large box shows the location of the interferograms used in this study. The main onshore active tectonic structures are drawn (barbed lines) from Armijo et al. (1996). (a) Model A: top of the fault at 4 km in depth. (b) Model B: top of the fault at 2.5 km in depth.

1995 campaign); May 1993 for points I, K, S, T, U, V, X, CU, CT102 and CT499 (processed using two softwares: GAMIT and the version 3.3 of the Bernese); September 1991 for points M, N, P, Q, R, C075 and C216 (processed using the GAMIT software).

To obtain a homogenous set of pre-earthquake coordinates, we corrected the measured pre-earthquake coordinates of each point for the long term motion, assuming a constant displacement rate before the event (vectors in Figure 10). For this purpose, we used the average displacement between 1991 and 1993 at each of the 14 points (A, B, C, D, E, G, I, K, M, S, T, U, V, X). The 1991–1993 data show a southern coast of the Gulf almost undeformed, and an average diplacement rate mostly independent of the site location on the northern coast, were all the points present an approximately northward motion at about 1.4 cm/year, except for point C (1.2 cm/year). This leads to a 4.5 cm opening of the rift between the 1991 campaign and the time of the Aigion earthquake.

The validity of the correction for the rift opening is confirmed by the small resulting vectors at the points located far from the epicentral area (A, G, I, N, K, V, X), their mean value being close to zero, and their r.m.s. scatter compatible with the 4 mm internal accuracy of individual campaigns (Figure 10). After correction, the residual displacement is interpreted as a coseismic displacement, mostly visible at points B, C, D, E, T, U, CU, C075, and CT499, and showing a N–S extension of about 10 cm between the two sides of the Gulf in centre of the deformed area. The much lower displace-

ments at points P, Q, R, S, CT, C216, and CT102 draws the limits of the fault plane. The isolated large displacement value at point M leads us to suspect a monument instability or local ground failure (soft soil site) and to reject this point. The internal accuracy for the vertical component of each GPS campaign (20 mm) and the different strategy applied for the tropospheric correction by Bernese and GAMIT limit, so far, our vertical accuracy in the range 40–70 mm for the comparison of two epochs. According to this value, the GPS data show a significant vertical change only at point C (144 mm of subsidence).

One interferogram was produced using two ERS1 SAR images taken on a descending track on 29 April 1995 and on 8 July 1995 (Figure 11, left). The altitude of ambiguity (Massonnet and Rabaute, 1993) of the interferogram is 130 m. The interferogram was obtained using a SPOT digital elevation model (DEM) whose accuracy is about 8 m. This value compared with the altitude of ambiguity of our interferogram ensures a sensitivity of the interferograms to errors in the DEM to be at most 1/20 of a fringe (28 mm), thus less than 2 mm in range. Probably due to the difference in the ground surface (limestone to the north, sediments and cultivated ground to the south), the coherence of the interferograms is good on the north side of the Gulf of Corinth and less in the south side but still enough to observe fringes if some were present. No fringe – or, conservatively, less than one fringe – is visible on the southern side of the Gulf of Corinth, thus excluding the Aigion fault as the major causative fault of the earthquake. Ten fringes are visible in the north side, near the GPS points C, C075 and C216, concentrated in an area of a few km centered around Psaromita cape. As the horizontal displacements deduced from GPS, mostly oriented N–S, do not significantly contribute to changes in SAR ranges (that are measured along a line almost E–W), and as in addition these displacements are moderate in this area, we conclude that these fringes are mainly created by vertical motion, consistent with the subsidence of point C seen by GPS.

We sampled one point every 0.5 to 1 km along each fringe of the interferogram. The 48 data (changes of range) were introduced in our inversion. Although the formal accuracy of the sampling of one point on one fringe is very low (2 mm), we further used a value of 40 mm for the accuracy of the motion obtained from the SAR data to avoid giving too much weight to these data which concern only one small part of the deformed area. The horizontal vectors deduced from the GPS measurements were introduced with accuracies of 5 mm. We used an inversion program (Briole et al., 1986) based on a least-square minimization algorithm developed by Tarantola and Valette (1982). The forward model assumes an uniform dislocation on a rectangular fault plane located in an elastic half-space (Okada, 1985), and is using 9 parameters per fault plane (Table 3).

A straightforward interpretation of the GPS data is that the northward motion of the points located above the hypocenter eliminates the possibility of a steep, south-dipping fault plane: in this case, these points would be on the hanging wall, and hence would move towards the south. We started our inversions assuming one single fault plane dipping north and leaving free the 3 angles (strike, dip, slip), fixing the hypocentral depth at 10 km. One stable solution was found by inversion, with a dip of 38°, a rake around $-80°$, and a strike around 275°: basically, smaller dip reduces the southward motion of the southern coast, and decreases the proportion between vertical and horizontal motion on the northern coast. However, the final dip is not in the acceptable range for the teleseismic data.

We therefore considered the largest dip, 35°, compatible with the teleseismic inversion, and the corresponding optimal strike, 275°, and an hypocentral depth of 10 km or larger, inverting for the fault dimensions. All best models exhibit a poor fit for the southern GPS points D and T ( the predicted motion is significantly less southward than the observation, and becomes even northward for D, because it lies in the influence zone of the hanging wall) and for the northern points C075 and CU (the predicted motion is less northward than the observation) (Model A, Figure 10a; best fit fault parameters in Table 3). We tried more complicated parametrizations around this model in order to improve the fit, dividing the fault into two or three segments along the NS direction, and inverting for the dip and north-south position of the shallow segment to the south. The latter segment always had the tendency to migrate northward during the inversion process, in order to drive points D and T away from the northward pull of the hanging wall, resulting in an unacceptable vertical superposition of the shallow and deep segments.

Good results with the dip constraint only appear when the hypocentral depth condition is relaxed: when the latter is less than 8 km in depth, a model with a single segment and a fixed dip angle of 35° provides a reasonably good final solution, with the top of the fault at 2.5 km in depth (Model B, Figure 10b; best fit fault parameters in Table 3); in particular, the southern

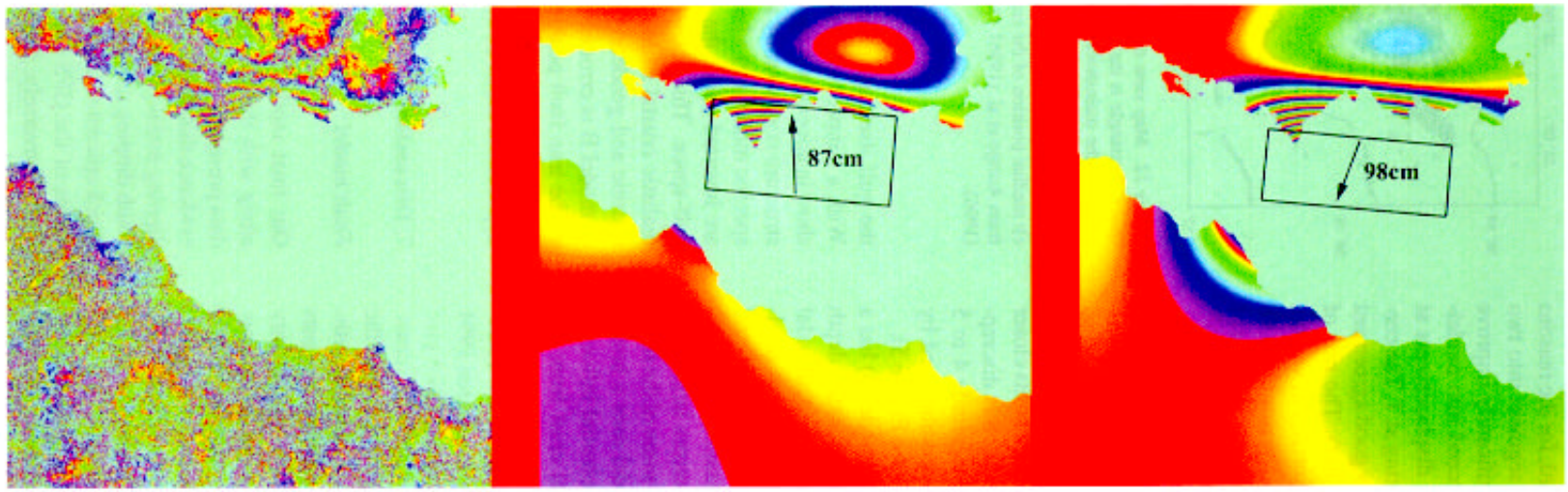


*Figure 11.* (left) Interferogram obtained by combining two ERS1 images taken on 29 April 1995 and 8 July 1995. The altitude of ambiguity is 130 m. Each fringe represents 28 mm. The error level is less than 2 mm. Ten fringes are visible around cape Psaromita on the north side of the Gulf. No fringes are visible in the southern side of the Gulf. (center) Synthetic interferogram obtained with model B (best fit GPS model of Figure 10b). (right) Synthetic interferogram obtained with a best-fit, south-dipping fault plane (see text).

points are correctly moving southward, for the reasons explained above. Splitting the fault segment into two independent segments does not significantly improve the fit; in particular, we did not succeed into modeling the westward component of the displacements at several points, the most significant being at T. The corresponding InSAR synthetic is in very good agreement with the InSAR data (Figure 11, center). The rms of the length of the 24 residuals GPS horizontal vectors after inversion is 16 mm for model B. The rms of the 48 SAR range residuals is 10 mm. The seismic moment of this solution is $3.9 \times 10^{18}$ N.m (rigidity $\mu = 3.3 \times 10^{10}$ N.m$^{-2}$). The slip on the fault is 0.87 m, the fault dimension is 9 km $\times$ 15 km. The InSAR data present about 1.5 fringe more than our best synthetic in the downgoing Psaromita cape (near point C), which might be due to unmodelled slip heterogeneity on the fault. The activation of one of the secondary offshore faults closer to the cape (see Figure 1) for explaining this discrepancy is less likely, as the shallow, magnitude 4 to 5 subevent that it would imply is not accompanied by any aftershock activity in its vicinity (see Figure 5).

This solution for a shallow source (model B) has a centroid at 5.1 km in depth and an hypocentral depth of 8 km, and is thus not consistent with the centroidal depth inferred from the teleseismic waveform modeling (range 6.0–7.5 km), nor with the hypocentral depth range imposed by the S-polarization at *serg* (> 10 km). This strongly suggests that errors larger than usually considered are introduced by some of the modeling procedures. As the Okada model uses a homogeneous half-space, we tested the potential influence of an important departure of the real crust from this assumption. Several observation sets indeed suggest the existence of a low rigidity shallow crust. The velocity structure of the Gulf deduced from the Aigion 1991 experiment (Rigo et al. (1996); Lemeur (1994)) give evidence for low-velocity, in the first 4 km of the crust, in particular on the sediments of the southern coast; the small incidence angles of first P-waves of local earthquakes for sites on both sides of the gulf also suggests low velocities in the shallowest crust (this low-velocity shallow crust has been considered in our teleseismic and local modeling). Furthermore, magneto-telluric sounding in the area reveals low resistivities (1-100 Ohm.m) of the first kilometer of the crust (Pham et al., (1996)), interpreted as an intense fracturation of the limestones to the north and a high porosity of the plio-quaternary sediments to the south, in both cases implying low rigidity. Finally, the thick sediments (possibly 2–3 km deep, according to Armijo et al., 1996) within the gulf itself are expected to have very low rigidity. With a simple two-dimensional elastic modeling, we show in appendix A that a normal fault in such a crustal structure is apparently shallower (by about 1 km in our specific modeling) when the true surface displacement are inverted under the assumption of a homogeneous half-space. This shows that one can succeed, with a realistic crustal structure, into reconciliating the teleseismic and geodetic data: we propose that the depth of model B is erroneous, resulting from the distortion of the true fault position by an oversimplified elastic model. Our preferred fault model is model A, with an hypocentral depth of 10 km.

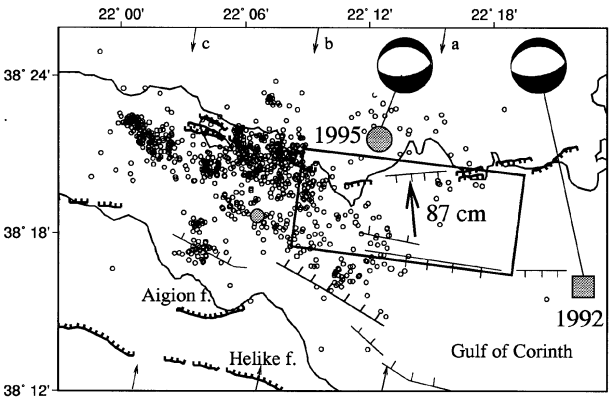


*Figure 12.* Map view of the final model of the 1995 Aigion earthquake. Rectangle is the fault projection at the surface. Large shaded dot is the mainshock epicenter. Small shaded dot is the main aftershock epicenter. Shaded square is the relocated 1992 Galaxidi epicenter. Circles: aftershocks as in Figure 4a. Arrows (a, b, and c): median position of the cross-section in Figure 5. Onshore faults from Armijo et al. (1996). Offshore faults from Papanikolaou et al. (1996).

## 7. Discussion

### *Fault model*

Our final model is presented in Figures 12 and 13, along with the aftershocks and the active faults. The data presented and analyzed above have provided clear evidence that the main activated fault plane is the north-dipping nodal plane of the teleseismic inversions. The south dipping normal fault plane containing the mainshock epicenter cannot explain the northward displacements of the GPS points of the northern coast of the gulf. Conversely, fitting this northward displacement with such a fault would imply to shift the epicenter

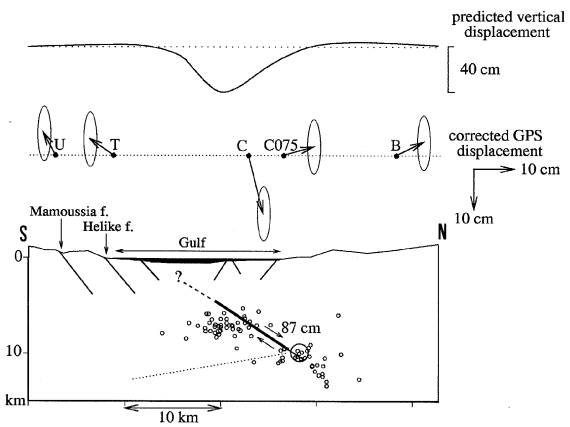


*Figure 13.* Cross-section of the final model (thick line in Figure 1). (top) Predicted vertical displacement (scaled to 0.87 m from Figure A2). (center) GPS inferred displacement vectors and error ellipses for the closest points to the profile. Note that as C is not located on the median profile (top), one cannot directly compare its downward motion with the calculated subsidence on the profile (top). (bottom) Thick line is the fault. Thin line is an unresolved continuation of the fault towards the hypocenter. Dashed line is an unresolved, possible upward continuation of the fault. Large circle is the hypocenter. Small circles are aftershocks (Figure 5a). Dotted line is the top of the low resistivity layer from Pham et al. (1996).

by at least 10 km to the south, which is well above the acceptable uncertainty in its location (2 km). The InSAR data are here not constraining by themselves: assuming a south-dipping fault plane, we could find a fault model providing a very good fit, as illustrated in Figure 11 (right); however, the associated hypocenter would be shifted by 8 km to the south, which is not acceptable. The absence of shallow aftershocks north of the northern coast is another element for ruling out a south-dipping normal fault cutting through the brittle, shallow pretertiary limestone of the area. The direction of extension is N $0^\circ \pm 5^\circ$, consistent with the results from Rigo et al. (1996).

The depth discrepancy between the best models obtained with the seismological data (A) and the geodetic data (B) has been resolved by assuming a low-rigidity shallow crust, which makes the geodetic inversion with a homogeneous half-space unsuitable. The true hypocentral depth is 10 km $\pm$ 1 km, consistent with teleseismic waveform modeling, hypocentral relocation with local and regional records, and S-wave local polarization. This result is further assessed by the fact that the upper continuation of fault model B cuts the ground surface in the middle of the gulf, where it cannot be connected to any of the north dipping faults scarps identified by Papanikolaou et al. (1996).

The second event appearing on the teleseismic source time function 6 s after the begining of the first event (Figure 7), if not an artifact, had a seismic moment about 20% of the total moment, and thus is of the order or less than $6 \times 10^{17}$ N.m, corresponding to a magnitude 5 or less. It would thus correspond to S accelerations of the order of or smaller than a few % of g at a distance of 10 km; an inspection of the *serg* and *aig* accelerograms (Figure 6) shows that such a source would not be detectable in the S-wave early coda of the first event. Such a source would also produce surface displacements of the order of 1 cm or less, remaining thus undetectable on GPS and inSAR data. There is thus no constraint in the location of the second subevent, if any.

The best-fit seismic moments inferred from GPS ($3.9 \times 10^{18}$ N.m) and waveform modeling ($3.4 \times 10^{18}$ N.m) are in good agreement; furthermore, if we consider a $35^\circ$ dip for the teleseismic inversion (to match the geodesy best-fit dip) we find $4.0 \times 10^{18}$ N.m, thus in excellent agreement with the geodesy. The HRV revised seismic moment is about 30% larger ($5.1 \times 10^{18}$ N.m). This might be due to a different parametrization of the structure in the source area: PREM model with ocean for HRV, Rigo et al.'s (1996) structure for our modeling.

The main rupture lasted 4 to 5 s, implying a mean rupture velocity of about $2.7 \pm 0.3$ km/s (80% of the shear-wave velocity), considering the 12 km length from the hypocenter to the furthest point of the activated fault plane. The directivity towards the south, deduced from the relative position of hypocenter and fault, and from the teleseismic inversion, is further assessed by the large acceleration (0.5 g) and the short duration (2 s) of the motion at *aig*, in the direction of the rupture (Figure 6).

The upper limit of the fault area is at about 4 km in depth under the median E–W axis of the gulf. The activated fault might be connected to the surface on a steeper plane (40–50°), reaching the sea-floor within the active submarine slumps detected on the southern, steep slope of the gulf by Papanikolaou et al. (1996): several active fault scarps have indeed been revealed on the bathymetric profiles within and at the bordures of these slumps (Figures 12). Although we cannot resolve the coseismic slip on this upper segment, which can range from 0 to a few tens of cm, we can reasonably propose that the main rupture stopped or became significantly less active when reaching the depth of about 4 km, thus possibly when entering within the thick sediments of the Gulf.

The coseismic subsidence by about 0.20 m of the sea floor averaged in an area of about 100 km$^2$, predicted by the geodetic model (see Figure 13), may explain the 0.5 m peak-to-peak tsunami observed in several places on the coast in the epicentral area and recorded by the NTUA/IPGP tide-gage near Galaxidi (P. Milas, personal communication). However, the coseismic occurrence of massive submarine landslides within the unstable areas delineated by Papanikolaou et al. (1996), suggested by the reports of metric subsidence of the shallow water sea-floor along new scarps typically a hundred meters long between the Aigion and the Helike fault (Ferentinos et al., 1996), may also have significantly contributed to this tsunami.

The distribution of the aftershock can be better interpreted within the proposed fault model. Its main characteristics is an intense activity to the west of the fault, and none to the east. We interpret this as the result of an increase in the Coulomb stress on both sides of the fault, which reaches a critical level to the west, but not to the east where the recent 1992 Galaxidi earthquake has released the local stress. We relocated the latter event simply by applying to its NEIC epicenter the same shift as for the 1995 mainshock NEIC epicenter (dotted squares and circles in Figure 4a). The resulting 1992 epicenter (shaded square in Figure 12) is a few kilometers east to the NOA determination, consistent with the shift observed for the 1995 NOA epicenter (see Figure 4a). Thus, the 1995 earthquake rupture stopped to the east near the western limit of the 1992 Galaxidi earthquake rupture zone.

*A low dip angle normal faulting*

Low-dip angle normal fault activity in the Corinth rift was already observed by Rietbrock et al. (1996), who accurately relocated a set of small normal fault events from a cluster 20 km west of the 1995 hypocenter, at a similar depth, possibly associated to the deepest part of the Psathopyrgos fault. These authors showed that the set of relocated hypocenters define a low-angle, north-dipping plane, consistent with one of the nodal planes of their focal mechanism, and suggesting the seismic activation of this plane by small-scale ruptures. Low-angle normal faulting might also have been the case for the 1992 Galaxidi earthquake ($M_s$=5.8), which had a similar depth and focal mechanism with a 30° northdipping nodal plane; however, we cannot reject the possibility of a rupture on the conjugate, southdipping plane.

Two mechanical models can be put forward for explaining this unusually low dip angle for normal faulting: a first model involves high fluid pressure such as those proposed for the San Andreas fault (Sibson, 1985; Rice, 1992), which may reduce the friction on such planes and allow a shear rupture, even for a vertical maximal stress at only 33° from the normal to the fault plane. The strong microseismic activity observed at some specific depths (Rigo et al., 1996; Hatzfeld et al., 1996; Figure 5, present study) indeed suggests large vertical variations in the strength or in the fluid pressures of some layers between 5 and 10 km in depth, possibly related to some of the stacked thrust nappes which compose most of the upper crust of the area (nappes of Gavrovo, Pinde, and Parnassos).

An alternative model involves the possibility of a non-vertical maximal compressive stress direction at the hypocentral depth (e.g., Bradshaw and Zoback (1988); Melosh (1990)). In the 1995 rupture area, this is suggested by the magneto-telluric profiles crossing the Aigion fault obtained by Pham et al. (1996), giving evidence for a highly conductive body below about 10 to 15 km in depth, and suggesting the presence of fluid-enriched crustal rocks and a ductile rheology. This layer, 5 to 10 km thick, seems to exist at a regional scale, not being confined to the center of the rift, and thus is probably inherited from the past thrust tectonics of the region. The interesting result for our concern is that in the source area of the Aigion 1995 earthquake, the top interface of this conductive layer apparently dips towards the south at an angle of about 10–15°: under the southern coast, the bottom depth of the resistive body is about 13 km, whereas under the northern coast, this depth reaches only about 10 km. Assuming that the conductive layer is ductile enough for relaxing the crustal tectonic shear stresses at the time scale of the seismic cycle, the top surface of this layer should contain one principal axis of the local stress tensor. We thus propose that the tension axis of the latter is dipping 10–15° to the south, matching the dip of the interface. In the source volume of the 1995 event, at about 10 km in depth, the tension stress axis would thus be at 43–58° from the 1995 fault plane, which is an acceptable value from the point of view of fracture mechanics and of Coulomb failure for normal faults.

The existence of this low-dip angle normal faulting in the western-central part of the rift remains however puzzling in the tectonic context of the gulf of Corinth described by Armijo et al. (1996). A steeper dip angle is indeed found for the Xilokastro fault, to the east of the Gulf: the 1981 earthquake (23 February) had a

$39^\circ \pm 10^\circ$ dip to the north according to Braunmiller and Nábělek (1996), consistent with the 40–60° dip angle deduced from the long term activity revealed by the tilting of uplifted marine terrasses and reversed drainage catchment (Armijo et al., 1996), and with the 1981 fault model by Hubert et al. (1996). To the south of the 1995 offshore fault, the Helike fault also presents a large and steep cumulative fault scarp, with uplifted plioquaternary sediments, similar to that of the Xilokastro fault, thus also suggesting large dip angles (see Figure 12 in Rigo et al. (1996)). Unfortunately, the terrasses for the Helike fault are much less developped, and their quantitative study by Rigo (1994) has not led to a well-constrained description of the long term fault activity nor of the morphology at depth. Therefore, we cannot exclude the possibility that the dip of the Helike fault reduces to less than 40° below 4–5 km in depth, thus presenting a similar geometry to that of the 1995 fault plane. In any case, the predicted vertical displacement of the 1995 rupture (Figure 13) does not fit the long term morphology of the rift: it creates almost no vertical uplift, and the subsiding area is shifted by about 3 km to the north with respect to the bathymetry. This suggests either that the associated fault is more rarely activated than the Helike fault, or that it has developped more recently.

Considering the similar faulting mechanisms of the 1965, 1970, 1992 and 1995 earthquakes, all of magnitude around 6 (Figure 1), one may suggest that the central part of the rift presents two modes of faulting, one with well-developped normal faults with rather long return period and large earthquakes (Helike type fault), and the other with possibly more frequent earthquakes with moderate magnitudes. This leads to two new, open questions for understanding the active tectonics of the rift: first, how significant is the contribution of such moderate earthquakes to the present opening of the rift, and, second, do they result from the rifting process itself, for instance by the crustal thining or flexure in the hanging wall of the major faults to the south, or do they occur on faults inherited from past tectonics?

## 8. Conclusion

We presented the results of a multidisciplinary study of the 1995, June 15, Aigion earthquake. We used all the available data from seismology (mainshock and aftershocks records on local, regional and teleseismic records), geodesy (GPS and SAR interferometry), and tectonics (mapping of surface breakage), for determining a first order model of the rupture geometry and kinematics.

Our best-fit model is the following (Table 3, model C): the rupture nucleated at 10 km in depth, 38° 21.7 N, 22° 12.0 E, which is 15 km NNE to the damaged city of Aigion, and propagated southward on a north-dipping, low dip angle (33°), offshore normal fault. Note that lacking the GPS measurements would have made quite impossible a proper choice between the two nodal planes of the teleseismic focal mechanism. For the modeling of geodetic data, it appeared that the effect of a low-rigidity shallow crust can be significant, and should be more carefully and systematically analyzed. The seismic moment inferred from GPS and InSAR data ($3.9 \times 10^{18}$ N.m) is 25% smaller than the HRV long period seismic moment, but consistent with that determined by inversion of the teleseismic body-waves. It provides a 0.87 m mean slip for fault area of 9 km $\times$ 15 km. The fault plane may be connected to the surface by a steeper segment cutting through the thick sediments of the gulf and reaching the sea-floor within the active submarine slumps on the southern slope. The aftershock seismicity is concentrated west of the rupture area, suggesting a crustal stress state closer to failure than to the east, relaxed by the 1992 Galaxidi earthquake.

Although some events were known to be good candidates for low angle normal faulting (Abers, 1991; Doser, 1987), this is the first well documented earthquake of this type (see Braunmiller and Nábělek (1996) for a critical discussion on seismological constraints for other alledged low angle continental normal faults). This unusual low-angle normal faulting may have been favoured by low-friction, high pore pressure fault zone, or, alternatively, by a rotation of the stress directions due to the possible dip towards the south of the mid-crustal, ductile layer. The similarity in focal mechanism and depth of this earthquake with other recent moderate earthquakes in the central part of the Gulf (1992, 1970, 1965) suggests for this area a faulting mechanism significantly different from that of the major normal faults outcropping near the southern coast of the rift, which exhibit more usual dip angles (40–50°). In any case, such low dip angle faulting under the norhern side of the Gulf cannot be the dominant cause for the long term morphology of the central part of the rift, suggesting a seldom, or recently started activity.

These results on the 1995 earthquake do significantly sharpen our perception of the seismic hazard

in the rift of Corinth. First, concerning the long term seismic hazard, as defined by tectonic studies, one should not only take into account the cumulative slip on the major faults borduring the southern coast inland, but also that of faults outcropping offshore, stressing the importance of detailed underwater exploration and geophysical prospection. Second, concerning the short term seismic hazard, the occurrence of the two recent moderate earthquakes (Aigion, 1995; Galaxidi, 1992) may have increased the probability of a large earthquake on the Aigion fault and possibly on the Psathopyrgos fault, but not on the Helike fault, most probably relaxed by the 1995 rupture. Finally, concerning the prediction of strong ground motion, the southern coast of the Gulf appears to be subject to a significantly higher seismic hazard than on the northern coast, not only due to softer sediments and the immediate proximity of major faults, but also due to directivity effects of the upward, southward ruptures to be expected for most of the large earthquakes there, as it was observed for the 1995 rupture in the city of Aigion.

## Appendix A

We show with a simple two-dimensional model the effect of a low-rigidity layer on surface displacements induced by a normal fault. The structure is presented in Figure A1. The low-rigidity, horizontal upper layer is 1.5 km thick, corresponding to the highly porous or fractured sediments in the Gulf area. The low-rigidity basin (triangle), 3 km deep, corresponds to the thick, weak sediments of the gulf itself. We assumed a low-rigidity value of 10% of the rigidity of the underlying medium. Using the finite elements code *Adeli* developped by Hassani (1994), we calculated the horizontal and vertical displacements for a normal fault with a top at 4 km in depth, under the deepest point of the basin, 9 km long, with a dip of 35°, thus similar to model A (Figure 10a). The results are presented in Figure A2, for three different structures: the model in Figure A1 (dashed line), the model without the triangular basin (dotted line), and a homogeneous half-space (solid line).

We first note that the vertical motion is mostly the same for the three structures. Most of the differences appear on the horizontal displacements: the horizontal layer alone generates a displacement increase of about 30%, and the additional effect of the basin is stronger to the south, due to its shorter distance, where at its peak it almost doubles the southward displacement with respect to a homogeneous half-space. Note also the northward shift of the maximal southward displacement when the low-rigidity layers are introduced. All these effects of the low-rigidity structure can be interpreted as an apparent smaller depth of the fault for an equivalent homogeneous model.

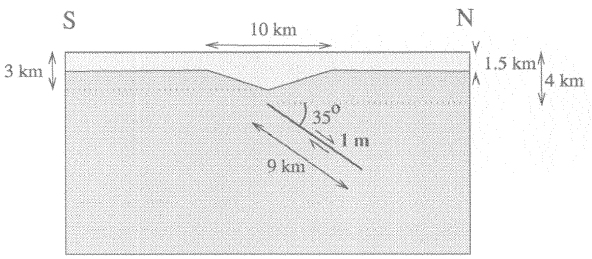


*Figure A1.* Two-dimensional (N–S cross-section) model of the rift. The light shaded area has a rigidity 10 times smaller than the dark shaded area. The triangular low-rigidity structure corresponds to the sediments of the gulf. The fault plane simulates the 1995 rupture, dipping 35° north.

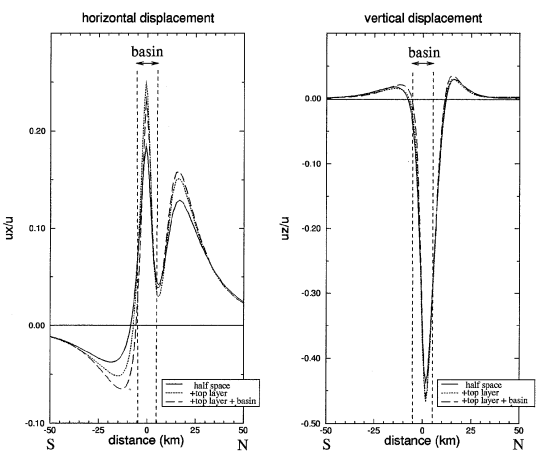


*Figure A2.* Horizontal and vertical surface displacements generated by the fault model of Figure A1, normalized to 1 m of slip on the fault, in a 2-D space. Solid line: elastic half-space. Dotted line: low-rigidity horizontal layer only over a homogeneous half-space. Dashed line: low-rigidity horizontal layer and triangular basin over a homogeneous half-space.

We tried to quantify this distorsion effect by inverting the horizontal displacements obtained with the basin structure, under the assumption of a homogeneous half-space. We fixed the dip of the fault (35°) and its length (9 km), leaving free its depth and position. The final, best fit fault is mostly vertically shifted, by 0.9 km upwards, with respect to the true fault.

In the case of the Aigion earthquake, we thus expect that the inversion of the GPS horizontal displacement

with the assumption of a homogeneous half-space will find a best-fit fault significantly shallower than the true fault. The precise amount of this vertical shift is yet impossible to estimate, and might be larger than the simple calculation presented above. Indeed, one should consider a 300 m layer of water with a zero rigidity, and a possibly 500 m thick, unconsolidated shallow sediments with neglectable rigidity, superimposed on the structure of Figure A1. These refined modeling, which would request a systematic study of the various parameters, are out of the scope of the present paper.

## Acknowledgments

We would like to thank here all the participants to the postseismic field work, N. Theodulidis (ITSAK), who provided us valuable informations for the aftershock records at *aig*. We are grateful to M. Nettles and G. Ekström for providing us a refined HRV focal mechanism solution. This work benefitted from the constructive criticisms of R. Armijo, J. Jackson and G.C.P. King. This work has been supported by CNRS/INSU (PNRN), and the CE Environment Program, Topic Seismic Risk (contract EV5V-CT94-0513). This is IPGP contribution no # 1481.

## References

Abers, G., 1991, Possible seismogenic shallow-dipping normal faults in the Woodlark-D'Entrecasteaux extensional province, Papua New Guinea, *Geology* **19**, 1205–1208.

Ambraseys, N. and Jackson, J., 1990, Seismicity and associated strain of Central Greece between 1890 and 1988, *Geophys. J. Int.* **101**, 663–708.

Armijo, R., Meyer, B., King, G., Rigo, A. and Papanastassiou, D., 1996, Quaternary evolution of the Corinth rift and its implications for the late Cenozoic evolution of the Aegean, *Geophys. J. Int.* **126**, 11–53.

Baker, C., Hatzfeld, D., Lyon-Caen, H., Papadimitriou, E., and Rigo, A., 1997, Earthquake mechanisms of the Adriatic sea and Western Greece, *Geophys. J. Int.*, in press.

Bernard, P. and Zollo, A., 1989, Inversion of near-source S polarization for parameters of double-couple point sources, *Bull. Seismol. Soc. Am.* **79**, 1779–1809.

Bernard, P., Herrero, A. and Berge, C., 1996, Modeling directivity of heterogeneous earthquake ruptures, *Bull. Seismol. Soc. Am.* **86**, 1149–1160.

Billiris, H., Paradissis, D., Veis, G., England, P., Featherstone, W., Parsons, B., Cross, P., Rands, P., Rayson, M., Sellers, P., Ashkenazi, V., Daavison, M., Jackson, J. and Ambraseys, N., 1991, Geodetic determination of tectonic deformation in Central Greece from 1900 to 1988, *Nature* **350**, 124–129.

Bouin, M.-P., Tellez, J. and Bernard, P., 1996, Seismic anisotropy around the Gulf of Corinth, Greece, deduced from three-component seismograms of local earthquakes and its relationship with crustal strain, *J. Geophys. Res.* **101**, 5797–5811.

Bradshaw, B. and Zoback, M., 1988, Listric normal faulting, stress refraction, and the state of stress in the Gulf Coast Basin, *Geology* **16**, 271–274.

Braunmiller, J. and Nábělek, J., 1996, Geometry of continental normal faults: seismological constraints, *J. Geophys. Res.* **101**, 3045–3052.

Briole, P., De Natale, G., Gaulon, R., Pingue, F. and Scarpa, R., 1986, Inversion of geodetic data and seismicity associated with the Friuli earthquake sequence (1976-1977), *Annales Geophysicae* **4**, 481–492.

Doser, D., 1987, The Ancash, Peru earthquake of 1946 November 10: evidence for low angle normal faulting in the high Andes of northern Peru, *Geophys. J. Roy. Astr. Soc.* **91**, 57–71.

Ferentinos, G., Koukis, G. and Papatheodorou, G., 1996, Subsea active faults in the W. Corintian gulf and subsea slides activated by the Egion earthquake of 15/6/1995, in *International Scientific Symposium, Earthquake, 6.1R, Egio earthquake*, extended abstract (in Greek), Aigion.

Hassani, R., 1994, Modelisation numerique de la deformation des systemes geologiques, These de l'Universite de Montpellier II.

Hatzfeld, D., Kementzetzidou, D., Karakostas, V., Ziazia, M., Nothard, S., Diagourtas, D., Deschamps, A., Karakaisis, G., Papadimitriou, P., Scordilis, M., Smith, R., Voulgaris, N., Kiratzi, S., Makropoulos, K., Bouin, M.-P. and Bernard, P., 1996, The Galaxidi earthquake of November 18, 1992: a possible asperity within the normal fault system of the Gulf of Corinth (Greece), *Bull. Seismol. Soc. Am.*, in press.

Herrero, A. and Bernard, P., 1994, A kinematic self-similar rupture process for earthquakes, *Bull. Seismol. Soc. Am.* **84**, 1216–1228.

Hubert, A., King, G., Armijo, R., Meyer, B. and Papanastasiou, D., 1996, Fault re-activation, stress interaction and rupture propagation of the 1981 Corinth earthquake sequence, *Earth Planet. Sci. Lett.* **142**, 573–585.

Jackson, J. J., Gagnepain, J., Houseman, G., King, G., Papadimitriou, P., Soufleris, P. and Virieux, J., 1982, Seismicity, normal faulting and the geomorphological development of the Gulf of Corinth (Greece): the Corinth earthquakes of February and March 1981, *Earth Planet. Sci. Lett.* **57**, 377–397.

Lemeur, H., 1994, Tomographie tridimensionnelle a partir des temps des premieres arrivees des ondes P et S, application a la region de Patras (Grece), These de Doctorat, Universite de Paris 7, France.

Massonnet, D. and Rabaute T., 1993, Radar interferometry: limits and potential, *IEEE Trans. Geosci. Rem. Sensing* **31**, 455–464.

Melosh, H. J., 1990, Mechanical basis for low-angle normal faulting in the Basin and Range province, *Nature* **343**, 331–335.

Mouyaris N., Papastamatiou, D. and Vita-Finzi, C., 1992, The Helice Fault, *Terra Nova* **4,** 124–129.

Nábělek, J., 1984, Determination of earthquake source parameters from inversion of body waves, PhD thesis, MIT, Cambridge, MA.

Nábělek, J., 1985, Geometry and mechanism of faulting of the 1980 El Asnam, Algeria, earthquake from inversion of Teleseismic body waves and comparison with field observations, *J. Geophys. Res.* **90,** 12,713–12,728.

Okada Y., 1985, Surface deformations due to shear and tensile faults in a half-space, *Bull. Seism. Soc. Am.* **75**, 1135–1154.

Papanikolaou, D., Chronis, G., Lykousis, V., Sakellariou, D. and Papoulia, I., 1996, Neotectonic structure of the W. Korinthiakos gulf and geodynamical phenomena induced by the Egion earthquake, in *International Scientific Symposium, Earthquake, 6.1R, Egio earthquake*, extended abstract (in Greek), Aigion.

Papazachos, B.C. and Papazachos, C. B., 1989, The earthquakes of Greece, Ziti Publications, Thessaloniki, Greece (in Greek).

Pham, V.N., Boyer, D., Chouliaras, G. and Bernard, P., 1996, Conductivité électrique et structure de la croûte dans la region du Golfe de Corinthe (Grèce) d'après les résultats de sondage magnétotellurique (SMT), *C. R. Acad. Sci. Paris.* **t.323,** 651–656.

Rice, J., 1992, Fault stress states, pore pressure distributions and the weakness of the San Andreas fault in Fault Mechanics and transport properties of rocks, ed. by Evans, B. and Wong, T. F., Academic Press, London, 475–503.

Rietbrock, A., Tiberi, C., Scherbaum, F. and Lyon-Caen, H., 1996, Seismic slip on a low angle normal fault in the Gulf of Corinth: evidence from high resolution cluster analysis of microearthquakes, *Geophys. Res. Lett.* **14,** 1817–1820.

Rigo, A., 1994, Etude sismotectonique et geodesique du Golfe de Corinthe (Grece), PhD thesis, Université Paris VII.

Rigo, A., Lyon-Caen, H., Armijo, R., Deschamps, A., Hatzfeld, D., Makropoulos, K., Papadimitriou, P. and Kassaras, I., 1996, A microseismic study in the western part of the Gulf of Corinth (Greece): Implications for large-scale normal faulting mechanisms, *Geophys. J. Int.* **126,** 663–688.

Rothacher M., Beutler G., Gurtner W., Brockmann E. and Mervart L., 1993, Bernese GPS Software Version 3.4 Documentation.

Sébrier, M., 1977, Tectonique recente d'une transversale a l'arc Egeen, these de doctorat, Universite Paris XI.

Schmidt, J. F. J., 1881, Studien uber Vulkans und Erdbeben, Leipzig.

Sibson, R., 1985, A note on fault reactivation, *J. Struct. Geol.* **7,** 751–754.

Tarantola, A. and Valette, B., 1982, Generalized nonlinear inverse problem solved using the least squares criterion, *Reviews Geophys.* **20,** 219–232.

Taymaz, T., Jackson, J. and Westaway, R., 1990, Earthquake mechanisms in the Hellenic Trench near Crete, *Geophys. J. Int.* **102,** 695–731.

Tselentis, G., Melis, N., Sokos, E. and Papatsimpa, K., 1996, The Egion June 15, 1995 (6.2 Ml) earthquake, Western Greece, *Pure App. Geophys.* **147**, 83–98.

Zollo, A. and Bernard, P., 1991, Fault mechanisms from near-source data: joint inversion of S polarizations and P polarities, *Geophys. J. Int* **104,** 441–451.